# Investigating Oxidative Addition Mechanisms of Allylic Electrophiles with Low-Valent Ni/Co Catalysts using Electroanalytical and Data Science Techniques

Tianhua Tang, Eli Jones, Thérèse Wild, Avijit Hazra, Shelley D. Minteer, and Matthew S. Sigman*

Department of Chemistry, University of Utah, 315 South 1400 East, Salt Lake City, Utah 84112, United States.

**ABSTRACT:** The catalysis by π-allyl-Co/Ni complex has drawn significant attention recently due to its distinct reactivity in reductive Co/Ni catalyzed allylation reactions. Despite significant success in reaction development, the critical oxidative addition mechanism to form the π-allyl-Co/Ni complex remains unclear. Herein, we present a study to investigate this process with four catalysis-relevant complexes: Co($^{Me}$BPy)$Br_2$, Co($^{Me}$Phen)$Br_2$, Ni($^{Me}$BPy)$Br_2$, and Ni($^{Me}$Phen)$Br_2$. Enabled by a electroanalytical platform, Co(I)/Ni(I) species were found responsible for the oxidative addition of allyl acetate. Kinetic features of different substrates were characterized through linear free-energy relationship (Hammett-type) studies, statistical modeling, and a DFT computational study. In this process, a coordination-ionization type transition state was proposed, sharing a similar feature with a Pd(0)-mediated oxidative addition in Tsuji-Trost reactions. Computational and ligand structural analysis studies support this mechanism, which should provide key information for next generation catalyst development.

## Introduction

Transition-metal catalyzed allylation-type reactions are a powerful method to construct new carbon-carbon and carbon-heteroatom bonds.[1] This class of reactions spans from palladium-catalyzed Tsuji-Trost reactions (Scheme 1a)[1] to more recent reductive allylation processes with first-row transition metals (Scheme 1b).[2–4] A common feature in all these transformations is the formation of a π-allyl-metal intermediate. Typically, a low-valent metal species undergoes oxidative addition across an allyl electrophile to generate a π-allyl-metal intermediate. Although this mechanistic event has been extensively studied for Pd(0) systems,[5–11] a similar mechanistic understanding of the oxidative addition process for Co or Ni systems has not been investigated in detail.[2]

The oxidative addition of Co(I)/Ni(I) species in reductive allylation performs two key functions in catalytic processes. Oxidation addition activates the allyl electrophiles, to provide access to the nucleophilic Co(II)/Ni(II) π-allyl intermediate (after a subsequent redox event). This intermediate then is proposed to engage in additions to various electrophiles.[3c,3e,4e,12,13] Understanding the intimate details of these steps will impact the further development of this emerging reaction class.

In contrast to the efforts in studying these events with Pd(0) complexes, studying the oxidative addition process of low-valent Co(I)/Ni(I) complexes has proven difficult. These complexes are typically unstable and are prone to speciation and disproportionation.[14,15] Sterically demanding ligands and specialized conditions are often required to stabilize these Co(I)/Ni(I) intermediates. This complexity is also manifested in measuring kinetic data, which is often needed to gain insight into the controlling events that influence catalysis.

To overcome several of these constraints, our groups[15–17] and others[18] have established an electroanalytical approach to studying oxidative addition processes of low-valent first-row transition metals across activated alkyl halides. Cyclic voltammetry (CV) studies simultaneously generate transient low-valent metal species and allow rapid access to rate data acquisition. This allows the application of physical organic studies, such as Hammett relationships and statistical modeling of the catalyst/substrate kinetics to provide valuable insight into the mechanism of substrate activation. More specifically, we have applied this method to elucidate the oxidative addition mechanisms for various first-row transition metal systems across *benzyl halide* substrates, where either halogen-atom abstraction or outer-sphere electron transfer mechanism was identified to be operating. (Scheme 1c).[15b,16]

Herein, we investigated four Co and Ni complexes bearing catalytically relevant ligands ($^{Me}$BPy, 6,6'-dimethyl-2,2'-bipyridine; $^{Me}$Phen, neocuproine) (Scheme 1c). During this process, we have identified a coordination-ionization type mechanism for activating allyl electrophiles in both Co(I) and Ni(I) systems. A comprehensive kinetic model relating structure to rate for a wide range of both catalysts/substrates was also constructed using multivariate linear-regression analysis. We believe that this mechanistic study could guide the rational design of future Co(I)/Ni(I) catalysis.

**Scheme 1. Mechanistic Studies of Oxidative Addition of Allyl Electrophiles**

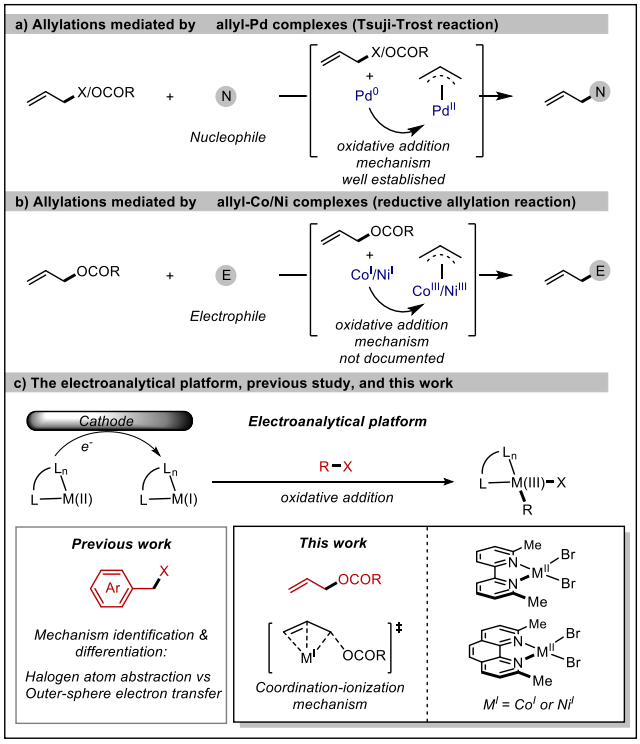


## Results and Discussion

**Electroanalytical Studies of the Co($^{Me}$BPy)Br$_2$, Co($^{Me}$Phen)Br$_2$, Ni($^{Me}$BPy)Br$_2$, and Ni($^{Me}$Phen)Br$_2$ Complexes and their Reactivity with Allyl Acetate.** Although different classes of bidentate ligands have been employed in Co/Ni catalyzed reductive allylation reactions, bipyridine- or phenanthroline-type ligands are the most common.[3c–d,3g,4b–c,4f–h] Thus, we initially focused on these two ligand classes in investigating Co(I)/Ni(I) oxidative addition process.

At the outset, we surveyed the cyclic voltammograms (CVs) of various Co/Ni complexes with phenanthroline and bipyridine-type ligands using acetonitrile solvent with $TBAPF_6$ as the supporting electrolyte. A considerable challenge in applying these ligands was the speciation of the metal complexes resulting in uninterpretable CVs with overlapping peak responses.[15] We hypothesized that placing methyl groups *ortho* to the nitrogen atoms of the ligands could increase the steric bulk of the metal center and minimize speciation issues through steric shielding of the complexes. Indeed, we found that $^{Me}$BPy (6,6'-dimethyl-2,2'-bipyridine) and $^{Me}$Phen (neocuproine) were effective ligands and provided quasi-reversible CVs. Particularly, both $^{Me}$BPy and $^{Me}$Phen have been previously shown to promote Co[19a–b] or Ni[4b,19c–g] catalyzed reductive coupling reactions.

Figure 1a–d depict the CVs of *in situ* prepared Co($^{Me}$BPy)Br$_2$, Co($^{Me}$Phen)Br$_2$, Ni($^{Me}$Phen)Br$_2$, and Ni($^{Me}$Phen)Br$_2$, measured at scan rates of 0.10 and 0.02 V s$^{-1}$. The geometry of either $Co^{II}X_2$ or $Ni^{II}X_2$ complex (X = Cl, Br, or I) bearing a bipyridine or phenanthroline-type ligand has been previously defined by crystallography as tetrahedron.[20] A boron-doped diamond electrode with a high overpotential for hydrogen evolution (−1.5 V in $H_2O$) was used for this analysis. The quasi-reversibility of these complexes allowed us to determine the redox potentials for M(II)/M(I) couples. We did observe an overlap of return peak responses for the Co($^{Me}$BPy)Br$_2$ complex (Figure 1a), which could arise from speciation of [Co$^{I}$($^{Me}$BPy)Br] and [Co$^{I}$($^{Me}$BPy)Br$_2^-$] complexes.[18] Additional voltametric studies of the speciation process are discussed in the supporting information (Section 5).

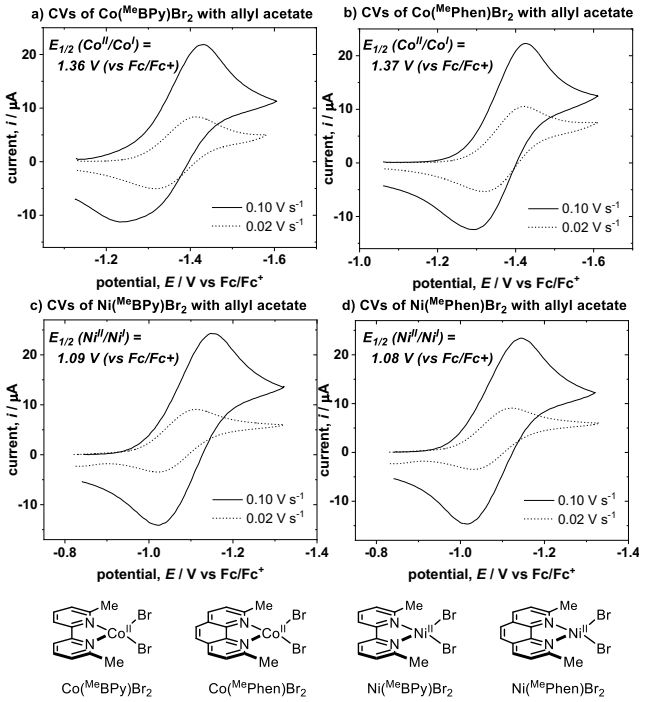


**Figure 1.** Representative CVs of (a) 1.0 mM $CoBr_2$ with 1.0 mM $^{Me}$BPy ligand, (b) 1.0 mM $CoBr_2$ with 1.0 mM $^{Me}$Phen ligand, (c) 1.0 mM $NiBr_2$·DME with 1.0 mM $^{Me}$BPy ligand, and (d) 1.0 mM $NiBr_2$·DME with 1.0 mM $^{Me}$Phen ligand at scan rates of 0.10 and 0.02 V/s in a 100 mM solution of $Bu_4NPF_6$ in acetonitrile, using a 0.071 cm$^2$ boron-doped diamond working electrode. All CVs are from the first scan.

To probe if these modified complexes are competent catalysts in a prototypical reductive allylation reaction, we conducted bulk electrolysis reactions with allyl acetate and benzaldehyde. Indeed, both cobalt and nickel complexes were able to catalyze the reaction (Table 1, entries 1−4). Control experiments revealed that Co/Ni complexes are necessary to promote the reactions ruling out direct electrolysis as a viable pathway (Table 1, entries 7 and 8). Interestingly, nickel bromide alone effectively catalyzes the reductive allylation, albeit in diminished yields (entry 5).

**Table 1. Bulk electrolysis reactions**

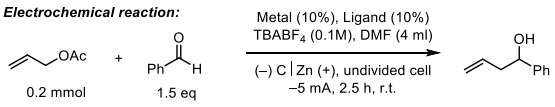


| entry | condition | yield (nmr) |
|---|---|---|
| 1 | $NiBr_2$ + $^{Me}$BPy | 40 |
| 2 | $NiBr_2$ + $^{Me}$Phen | 41 |
| 3 | $CoBr_2$ + $^{Me}$BPy | 61 |
| 4 | $CoBr_2$ + $^{Me}$Phen | 60 |
| 5 | $NiBr_2$ / no lig | 29 |
| 6 | $CoBr_2$ / no lig | 0 |
| 7 | $^{Me}$BPy / no metal | 0 |
| 8 | $^{Me}$Phen / no metal | 0 |

[a]Conditions: 0.2 mmol allyl acetate, 1.5 equiv. benzaldehyde, and 0.1 M $TBABF_4$ in 4 ml DMF, Zn anode, carbon felt cathode, undivided cell, and electrolysis at room

temperature under a constant current of 5 mA for 2.5 h. The metal salt and ligand are specified in the table. Yield was determined by $^1$H NMR with trimethoxybenzene as the internal standard.

Next, we investigated the reactivity of a transiently generated Co(I)/Ni(I) complexes with allyl acetate as the substrate using CV. Upon addition of 1.0 and greater equivalents of allyl acetate, the cyclic voltammograms of all four Co/Ni complexes showed partial loss of reversibility (Figure 2a–d): the return peak in each CV decreased in the current while no noticeable change in the forward peak was observed. This is consistent with the interception of electrogenerated Co(I)/Ni(I) species by allyl acetate, indicative of an oxidative addition process.[3g,12b,16–18] Similar reactivity has been previously proposed for Co(I) complexes in stoichiometric studies.[3e,3g] However, for the Ni-catalyzed reductive coupling reactions, both Ni(0)/Ni(II)[4b,4e–h,13] and Ni(I)/Ni(III)[4c,21] catalytic cycles were proposed to be operative. While not ruling out a Ni(0)/Ni(II) catalytic cycle, our cyclic voltammetry studies indicated that Ni(I)-mediated oxidative addition is a viable pathway for the reductive couplings using the ligands under investigation. As a result, the CV patterns can be interpreted as an EC-type mechanism (electrochemical reduction, 'E,' followed by a chemical step of Co(I) or Ni(I)'s oxidative addition into allyl acetate, 'C,' Figure 2e).

The rate constants for the chemical step in the EC mechanism were determined using peak-ratio analysis, a method established by our previous work[15–17] and Liu and Diao's recent report.[18] For a detailed discussion on the theoretical foundation as well as derivatization process, we direct readers to the supporting information (Section 2). We found that Ni(I) complexes were twice as reactive as the cobalt complexes (Table 2), although cobalt complexes were more reducing than the nickel complexes (−1.36 V vs −1.09 V). Additionally, the $^{Me}$Phen ligand facilitated the oxidative addition process for Co and Ni compared to $^{Me}$BPy, despite no significant difference in redox potentials of the $^{Me}$BPy and $^{Me}$Phen complexes. These observations suggest the oxidative addition rate does not directly depend on the reducing ability of the complex.

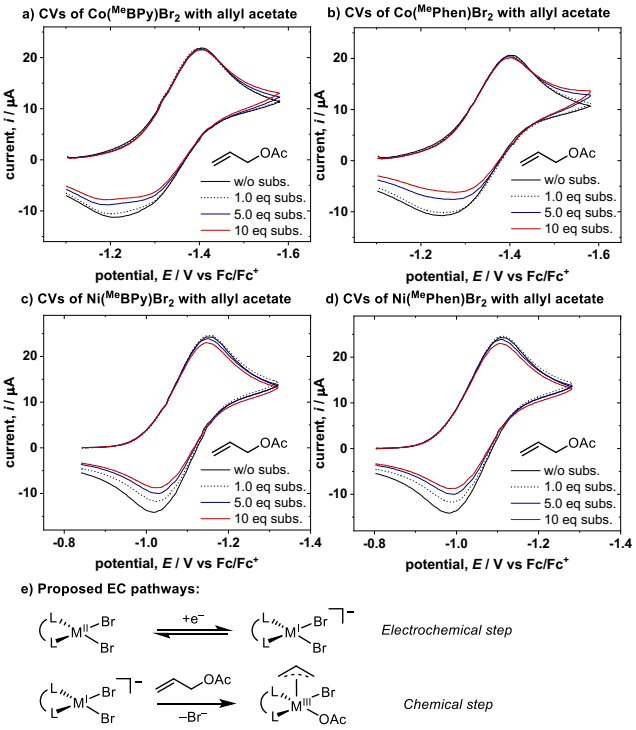


**Figure 2.** CVs run at varying equivalents of allyl acetate (0, 1.0, 5.0, and 10 equiv.) with (a) 1.0 mM $CoBr_2$ with 1.0 mM $^{Me}$BPy ligand, (b) 1.0 mM $CoBr_2$ with 1.0 mM $^{Me}$Phen ligand, (c) 1.0 mM $NiBr_2$·DME with 1.0 mM $^{Me}$BPy ligand, and (d) 1.0 mM $NiBr_2$·DME with 1.0 mM $^{Me}$Phen ligand at the scan rate of 0.10 V/s in a 100 mM solution of $Bu_4NPF_6$ in acetonitrile, using a 0.071 cm$^2$ boron-doped diamond working electrode. (e) Proposed EC mechanism. All CVs are from the first scan.

**Table 2. Tabulated redox potential, rate constants (with allyl acetate), and derived activation energy[a]**

| *Investigated complex* | *Co($^{Me}$BPy)Br$_2$* | *Co($^{Me}$Phen)Br$_2$* | *Ni($^{Me}$BPy)Br$_2$* | *Ni($^{Me}$Phen)Br$_2$* |
|---|---|---|---|---|
| *$E_{M(I)/M(II)}$ (V vs Fc/Fc$^+$)* | *1.36* | *1.37* | *1.09* | *1.08* |
| *$k_{(M(I)\ +\ allyl\ acetate)}$ (dm$^3$ mol$^{-1}$ s$^{-1}$)* | *5.4* | *12.6* | *16.0* | *24.7* |
| *$G^{\ddagger}$(exp) (kcal/mol)* | *20.6* | *20.0* | *19.9* | *19.6* |

[a]Redox potential $E_{M(I)/M(II)}$ was determined by CV and rate constant $k_{((M(I)+allyl\ acetate)}$ was determined using peak-ratio analysis. Activation energy ($\Delta G^{\ddagger}$) was calculated by Eyring equation.

**Linear Free-Energy Relationship (Hammett-type) Study.** To investigate the mechanism of oxidative addition, we conducted a kinetic analysis through a linear free-energy relationship (Hammett-type) study.[15–16] Substrates bearing different aryl substituents, whose electronic properties can be easily manipulated and characterized by Hammett parameters ($\sigma$),[22] were prepared and classified into 4 different types: (1) C1−substrates bearing different aryl groups on the alkene's terminal position (Figure 3a, substrate **1**–**12**); (2) C2−substrates bearing different aryl groups on the alkene's internal position (Figure 3b, substrate **13**–**20**); (3) C3−substrates bearing different aryl groups on the allylic position (Figure 3c, substrate **21**–**31**); (4) C4−substrates bearing different benzoate groups (Figure 3d, substrate

**32**–**42**). The relative rate constants for oxidative addition of Co(I)/Ni(I) complexes across various substrates were measured and the resulting Hammett-type analysis is summarized in Figure 3.

Hammett plots for C1– and C2–substrates (Figures 3a and 3b) display a linear trend with positive $\rho$ values for all complexes, suggesting a negative charge build-up on the alkenyl positions during the transition state. Electron-deficient alkenes with better π-coordination reacted faster, suggesting pre-coordination of the Co(I)/Ni(I) complexes to the alkene component during oxidative addition.

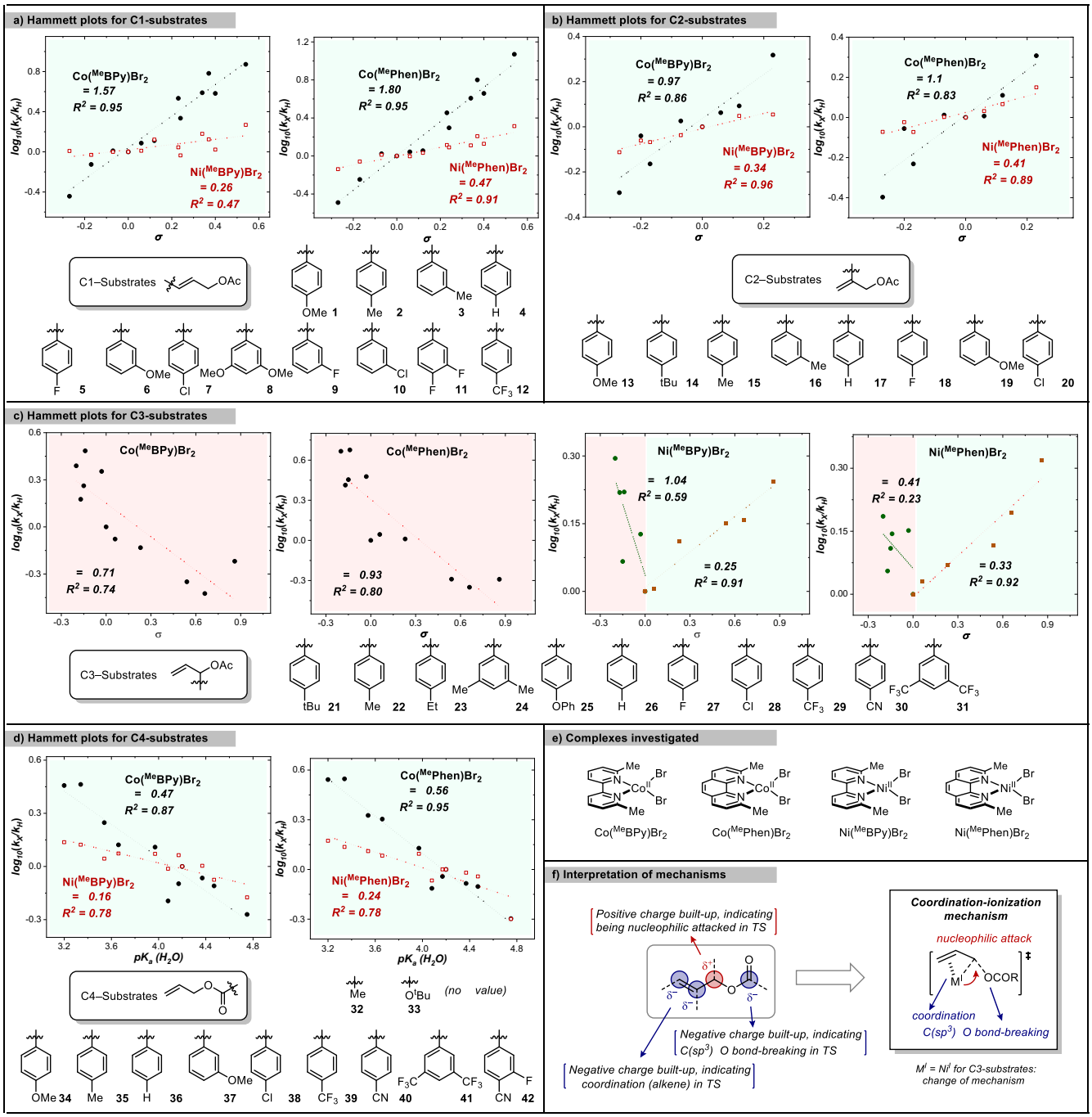


**Figure 3**. Linear free-energy relationship (Hammett-type) study of oxidative addition reactions with all four Co and Ni complexes: Correlation of σ parameters or $pK_a$ values to kinetic data from (a) C1-substrates (**1**–**12**), (b) C2-substrates (**13**–**20**), (c) C3-substrates (**21**–**31**), and (d) C4-substrates (**32**–**42**). (e) Investigated complexes. (f) Interpretation of mechanisms. σ values are from ref. 22, and $pK_a$ values are converted from $\sigma$ values.

C3–substrates for Co/Ni complexes displayed distinct Hammett patterns (Figure 3c). We observed a negative ρ value for cobalt complexes, indicative of a positive charge build-up on the allylic position during the transition state. This could be interpreted as a nucleophilic attack[23] of the allylic carbon by Co(I), and a similar trend was previously reported for an Fe-mediated oxidative addition process through a nucleophilic substitution ($S_N2$) mechanism.[24] Intriguingly, a broken

Hammett plot was observed for the nickel complexes where both electron-deficient and electron-rich substrates accelerated the oxidative addition process. We postulated this could indicate a change of mechanism in switching from electron-rich (**21**–**25**) to electron-poor (**27**–**31**) substrates.[25] For electron-rich substrates, a negative correlation could be indicative of a nucleophilic attack by Ni(I), consistent with the reactivity of Co(I). A positive correlation, in contrast, is more difficult to interpret. In previous reports[14b,26] of aryl halide oxidative addition, a positive correlation was interpreted as a three-centered concerted pathway. A similar Hammett trend in alkyl halide activation was used to support a single electron transfer (SET) pathway.[15,16,18] Although not conclusive, we believe the additional radical stabilization of allylic position by the aryl group points towards a SET pathway for the electron-deficient C3−substrates.

Finally, rates for C4−substrate were examined through a correlation of the $pK_a$ value of the conjugate acid of the carboxylate (Figure 3c) to create a Brønsted-type plot. This allowed us to incorporate substrates that lack Hammett parameters (allyl acetate **32** and allyl *t*-butyl carbonate **33**). A negative correlation to $pK_a$ was found for all four complexes, suggesting that a better leaving group ability facilitated the oxidative addition. These results are consistent with the breaking of C($sp^3$)−O bond in the transition state, similar to a trend previously observed for a Pd(0)-mediated process.[9]

In summary, a general mechanism initiated by π-coordination of the substrate with Co(I)/Ni(I) complexes (Figure 3e) occurs. Subsequently, the metal attacks the allylic position although a SET pathway is possible for Ni(I) complexes with electron-deficient C3−substrates (**27**–**31**) with concomitant C($sp^3$)−O bond-breakage during oxidative addition. Taken together, a general coordination-ionization type transition state is proposed (depicted in Figure 3f). This is a similar mechanism to those proposed for Pd(0)[5,7] or Ni(0)[27] mediated processes in Tsuji-Trost reactions. Significant mechanistic contrast has been reported for the oxidative addition of organic substrates between Co(I)/Ni(I) and Pd(0)/Ni(0) systems.[28] Therefore, it is intriguing that our study corroborates shared features in these two systems for the oxidative addition of allyl esters.

**Parameterization of Substrates and Statistical Modeling of Kinetic Data.** In order to integrate and compare the rate profiling more effectively, we applied multivariate linear-regression (MLR) analysis.[29] The MLR workflow has two essential components: (1) acquisition of rate data from a diverse set of substrates, and (2) extraction of structural properties that can be described by molecular parameters. Statistical models with a correlation between rates and these parameters can then be constructed and utilized to interpret mechanism. Thus, we combined all the measured rate data from C1, C2, C3, and C4−substrate classes using the two different ligands with each metal source to build a statistical model. For molecular descriptors, we chose the natural bond orbital (NBO) charges of the core carbons of the allylic substrate and the $pK_a$ (acidity of carboxylate, experimental values), which might describe the transition state features identified in Hammett-type studies. To utilize the two different ligands, a binary classifier was included.

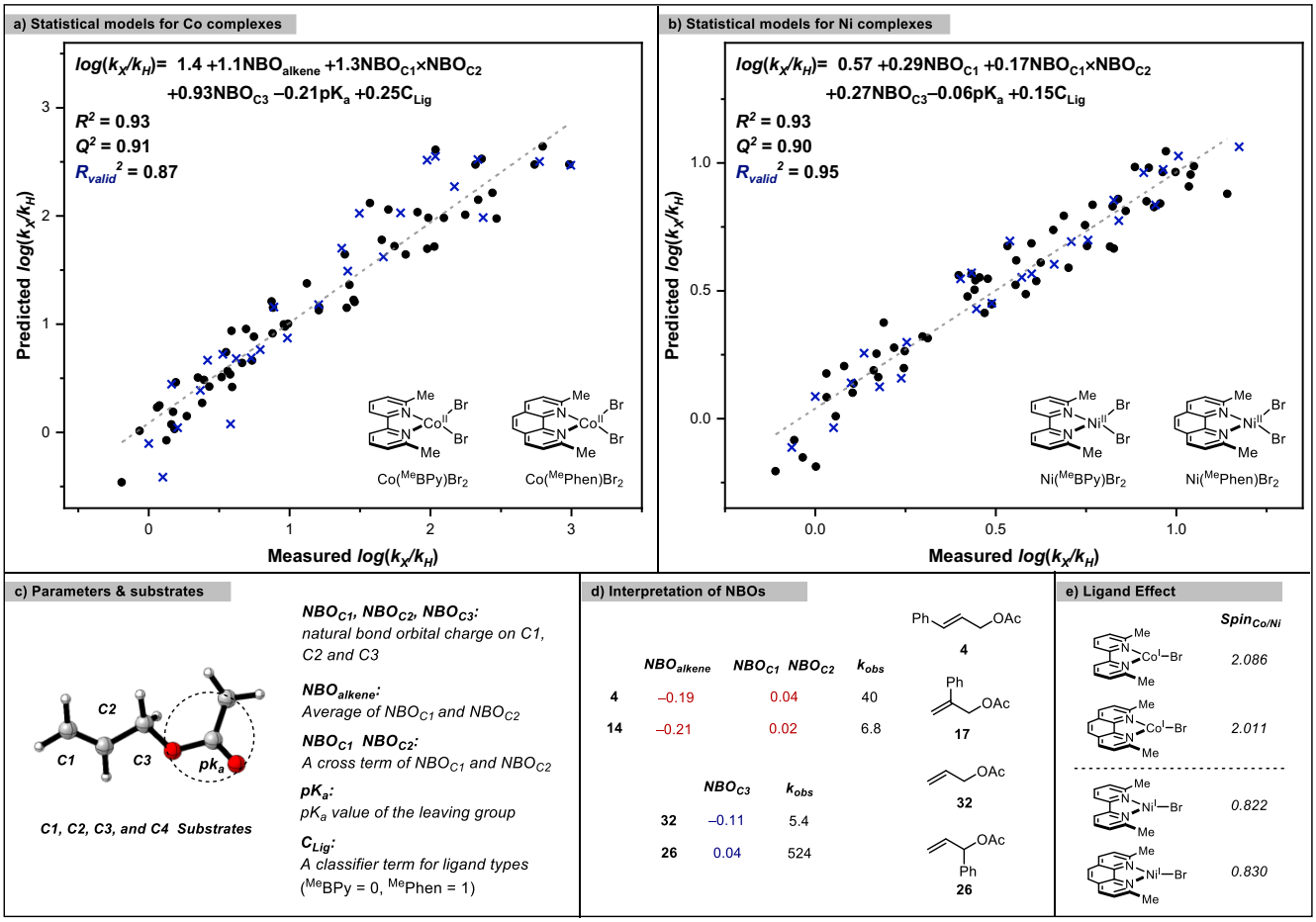

**Figure 4.** Multivariate linear regression analysis of substrates' kinetic data for (a) two cobalt complexes and (b) two nickel complexes with a pseudo-random 70:30 split into training/validation data set (black circle: training set, blue cross: validation set). (c) Description of substrate parameters and classes used in the models. (d) Interpretation of NBO parameters using $k_{obs}$ from Co($^{Me}$BPy) to exemplify. (e) A rational for observed ligand effect using $Spin_{Co/Ni}$ (Spin density on the $Co^{I}$ or $Ni^{I}$ center).

A pseudo-random split of the data into training and validation sets (70:30 split) was performed on the entire data set for both metals (84 rates for Co and 83 for Ni). Utilizing the parameters mentioned above, forward stepwise linear regression analysis was performed incorporating individual descriptors as well as cross-terms. Robust models were found for both Co and Ni with excellent internal and external validation statistics ($R^2$, $Q^2$ (leave-one-out validation coefficient), and $R_{valid}^2$ are >0.85 in each model, depicted in Figure 4a and 4b). Specifically, five parameters (Figure 4c) were found to correlate: (1) $NBO_{alkene}$ (in Co model): the average of the NBO charge on both alkenyl carbons (C1 and C2), or $NBO_{C1}$ (in Ni model): NBO charge on C1 position; (2) $NBO_{C1}\times NBO_{C2}$: a cross-term of the $NBO_{C1}$ and $NBO_{C2}$; (3) $NBO_{C3}$: NBO charge on allylic position (4) $pK_a$: the experimental value of the carboxylates; (5) $C_{Lig}$: a classifier term for ligands ($^{Me}$BPy as 0, $^{Me}$Phen as 1). The correlation with the two alkene and one allylic NBO terms indicate that electron density on the alkenyl and allylic positions significantly impacts the observed rate. We reasoned that the alkenyl carbons with less electron density increase the rate indicates a pre-coordination with metal complex. The charge stabilization on the allylic position, characterized by $NBO_{C3}$, on the other hand, indicates a nucleophilic attack by metal. As tabulated in Figure 4d, substrate **4** with a larger value in either parameter is more reactive than **17**. Substrate **26** is more reactive than **32** because **26** has a larger NBO charge on the allylic position. In addition, the negative coefficient associated with the $pK_a$ parameter suggests that the oxidative addition is facilitated by the feasibility of the C–O bond-breaking process. Lastly, $^{Me}$Phen's rates are generally faster than $^{Me}$BPy as quantified by the $C_{Lig}$ term. For rationalization of this ligand effect, we provide a hypothesis using DFT-derived features. The $^{Me}$Phen complex has a larger spin density on the metal than the $^{Me}$BPy complex, which could result in a more reactive metal center and thus faster oxidative addition (Figure 4e).

Aligned with our Hammett-type studies, the statistical models support a coordination-ionization type transition state. However, the apparent change of mechanism, observed for C3-substrates in Ni's Hammett plots, is not captured in the MLR models.

**Kinetic and Synthetic Studies on methylated allylic substrates.** Further validation of the coordination-ionization type mechanism was obtained by measuring the rate constants of different methyl substituted allyl acetates. These types of substrates have proven beneficial to uncovering the mechanism for the Pd(0)-catalyzed Tsuji-Trost reactions,[8] which share a similar proposed mechanism with ours. As summarized in Table 3, addition of a methyl group on the C1 or C2 alkenyl position slowed the oxidative addition rates while C3 substituted allyl chlorides showed enhanced rates.[8b]

To explore a similar analysis, we prepared a series of allyl ester substrates **39**, **43**–**48** bearing methyl substituents on different positions (both alkenyl and allylic) and measured their rate constants with all four Co(I) and Ni(I) complexes (Table 3). Compared to substrate **39**, methyl substituents decreased the rate when on the alkenyl positions (**43**–**46**) but increased the rate when appended to the allylic positions (**47**–**48**). This is in accordance with the rate trends observed with Pd(0) and thus further supports a coordination-ionization mechanism for the Co(I)/Ni(I) systems. Specifically, methyl substituents on the alkenyl carbons slow the coordination to the metal while methyl groups on the allylic position stabilize the resultant positive charge build-up during the metal's attack possibly with an $S_N1$ feature.

**Table 3. Methyl Effect for a previously reported Pd(0) system[8b] and the Co(I)/Ni(I) systems**

| $k_{rel}$ | Pd– | $k_{rel}$ | Co($^{Me}$BPy)$Br_2$ | Ni($^{Me}$BPy)$Br_2$ |
|---|---|---|---|---|
| Cl | 1 | OCOAr 39 | 1 | 1 |
| Me, Cl, Me | 0.32 | Me, OCOAr, Me 43 | n.r.[a] | n.r.[a] |
| Cl, Me | n.d. | OCOAr, Me 44 | n.r.[a] | n.r.[a] |
| Me, Cl | 0.13 | Me, OCOAr 45 | 0.21 0.03 | 0.28 0.01 |
| Me, Cl | 0.22 | Me, OCOAr 46 | 0.14 0.01 | 0.67 0.01 |
| Cl, Me | 1.5 | OCOAr, Me 47 | 1.4 0.04 | 1.9 0.01 |
| Cl, Me, Me | n.d. | OCOAr, Me, Me 48 | 3.0 0.10 | 4.5 0.10 |

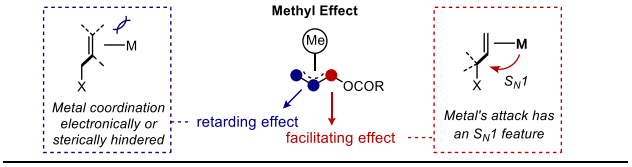


[a]n.r., no reaction observed. Error bars were calculated on duplicated measurements. The Co or Ni($^{Me}$Phen) systems show similarity with $^{Me}$BPy systems, and are reported in the supporting information (Section 7). Ar = 4-$CF_3$-phenyl.

The similarity between Pd(0) and Co(I)/Ni(I) systems was also observed in catalytic coupling reactions. π-allyl-Pd complexes have previously been shown to rapidly isomerize and generate the same isomeric products irrespective of the substitution pattern/geometry of the starting material (depicted in Figure 5).[10]

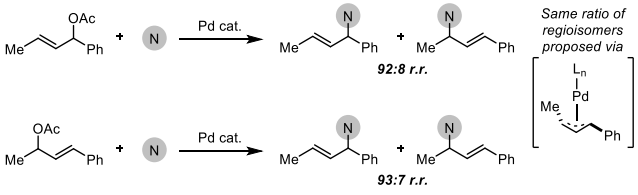


**Figure 5.** Isomerization of π-allyl-Pd complex leading to same ratio of regioisomers from different substrates (ref.10b). N = nucleophile.

To determine if this pattern of reactivity is also shared with Co(I)/Ni(I) systems, we treated methylated substrates (**39**, **43**–**45** and **47**–**48**) with benzaldehyde as the electrophile using modified conditions from those described above. As depicted in Table 4, Co($^{Me}$BPy)$Br_2$ catalyzed reactions were achieved with fair to good yields (44–63%) of products but poor diastereoselectivity (entry 2). Interestingly, isomeric allyl esters in entries 2 and 3 produced the same single regioisomers indicating isomerization of the π-allyl-metal species prior to the coupling event (Entry 4). Similar trends were observed for Ni($^{Me}$BPy)$Br_2$ catalyzed reactions (see supporting information, section 12). In both entries 2 and 3, the newly formed bond was at the more substituted carbon, consistent with several previous reports on reductive Co/Ni catalyzed allylation reactions.[3c–e,4a,30]

**Table 4. Electrochemical control experiments**

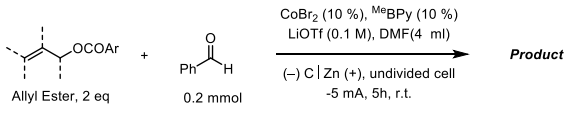


| Entry | Allyl Ester | Product | %Yield (d.r.) |
|---|---|---|---|
| 1 | unsubstituted |  | 63 |
| 2 | mono-methyl substituted | 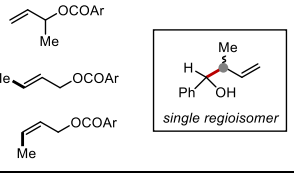 single regioisomer | 44 (1.0:1 d.r.)<br>52 (1:1.1 d.r.)<br>49 (1.1:1 d.r.) |
| 3 | gem-di-methyl substituted | 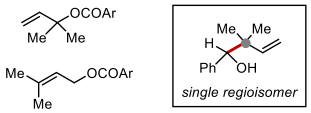 single regioisomer | 53<br>52 |
| 4 | Mechanistic interpretation |  | |

[a]Conditions: 0.2 mmol benzaldehyde, 2.0 equiv. allyl esters specified in the table, 0.02 mmol $CoBr_2$, 0.02 mmol $^{Me}$BPy, and 0.1 M LiOTf in 4 ml DMF, Zn anode, carbon felt cathode, undivided cell. Electrolysis at room temperature under a constant current of 5 mA for 5 h. Yield was determined by isolation. Ar = 4-$CF_3$-phenyl.

**Evaluating Electronic and Steric Effects of Co/Ni Complexes.** To better understand how ligand variation impacts oxidative addition rates, we prepared several Co or Ni complexes bearing electronically and sterically demanding bipyridine-type ligands (**L1**–**L7**) and phenanthroline-type ligands (**L8**–**L13**).

For bipyridine-type ligands, **L1**–**L4** possess different electronic properties (from electron-rich to electron-poor), while **L5** has sterically hindered substituents on the 6,6'-positions. **L6** and **L7** bear phenyl substituents on either *ortho* or *para* positions. The redox potential and rate constant (with substrate **39**) for each complex were determined (Table 5). The CVs of Co(**L1**)$Br_2$, Co(**L5**)$Br_2$, Co(**L6**)$Br_2$, Co(**L7**)$Br_2$, Ni(**L6**)$Br_2$, and Ni(**L7**)$Br_2$ showed complex cyclic voltammetry behavior and have therefore been excluded from this analysis (see supporting information, section 11). The remainder of the complexes gave interpretable CVs, although oxidative addition was too slow to be measured with either Ni(**L4**)$Br_2$ or Ni(**L5**)$Br_2$ complexes. Generally, the oxidative addition process is typically faster for both Co and Ni complexes bearing electron-donating ligands consistent with the redox potentials of these complexes. While ligand size is difficult to quantify for the cobalt complexes, nickel complex Ni(**L5**)$Br_2$, which contains bulkier 6,6'–substituents, significantly slowed the rate of oxidative addition presumably due to hindered interaction of the substrate. Moreover, the chlorinated and brominated complexes (Co(**L3**)$Cl_2$ and Co(**L3**)$Br_2$, or Ni(**L3**)$Cl_2$ and Ni(**L3**)$Br_2$) give similar rates although the chlorinated complex has a more negative redox potential. Though an investigation on oxidative addition by complexes bearing phenyl-substituted ligands (**L6** and **L7**) was difficult, we found these complexes possess less negative redox potentials, which may further slow oxidative addition.

**Table 5. BPy ligands' electronic and steric effects.**

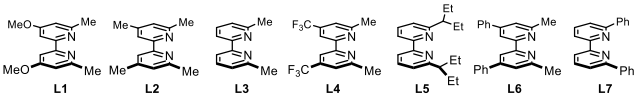


| $L_X$ | $Co(L_X)Br_2$ | | $Ni(L_X)Br_2$ | |
|---|---|---|---|---|
| | $E_{1/2}$ /V | $k_{obs}$ / $M^{-1}$ $s^{-1}$ | $E_{1/2}$ /V | $k_{obs}$ / $M^{-1}$ $s^{-1}$ |
| L1 | –1.53 | n.d.[a] | –1.15 | 34.0 0.5 |
| L2 | –1.45 | 42.9 2.1 | –1.11 | 31.7 0.2 |
| L3 | **1.36** | **13.2 0.4** | **1.10** | **21.7 0.3** |
| L4 | –1.04 | 1.51 0.21 | –0.94 | n.r.[b] |
| L5 | –1.38 | n.d.[a] | –1.11 | n.r.[b] |
| L6 | –1.32 | n.d.[a] | –1.05 | n.d.[a] |
| L7 | –1.16 | n.d.[a] | –1.00 | n.d.[a] |
| $M(L_3)Cl_2$ | –1.49 | 10.5 1.2 | –1.21 | 20.1 0.2 |

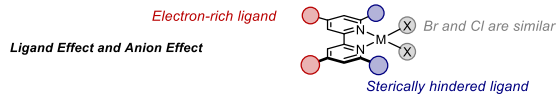


Kinetic rate constants (with **39**) and redox potentials (referenced to $Fc/Fc^+$) were measured and compared between nickel and cobalt complexes bearing different ligands. [a]Rate constants not determined due to uninterpretable CVs. [b]No observation of reactivity. Error bars were calculated on duplicated measurements.

For phenathroline-type ligands, **L8**–**L11** possess different electronic properties (from electron-rich to electron-poor), while **L11** has hindered substituents (n-butyl). **L12** and **L13** bear phenyl substituents on either *ortho* or *para* positions (to the nitrogen atoms). In a similar manner as above, the electrochemical properties and oxidative addition rate constants were determined and tabulated in Table 6. Overall, the electronic effect of Co-promoted oxidative addition was difficult to analyze due to uninterpretable CVs of both Co(**L8**)$Br_2$ and Co(**L10**)$Br_2$ (see supporting information, section

11). However, for Ni complexes, an electron-rich ligand (**L8**) was found to facilitate oxidative addition while an electron-poor ligand (**L10**) slowed the process. Interestingly, the opposite effect was observed for Co and Ni when using a sterically demanding ligand (**L9** *vs* **L11**) wherein an increase in rate is observed using Co compared to a slowing in rate for the Ni species. The oxidative addition were also studied for chlorinated complexes (M(**L$_9$**)Cl$_2$), which show a different rate from the brominated complexes (M(**L$_9$**)Br$_2$). Moreover, for both Co and Ni, complexes bearing *para*-phenylated ligands (**L9** *vs* **L12**) possess less negative redox potentials and slow oxidative addition. However, complexes bearing **L13** with less negative redox potentials (*vs* **L9**) were not compatible with rate analysis due to uninterpretable CVs.

**Table 6. Phen ligands' electronic and steric effects.**

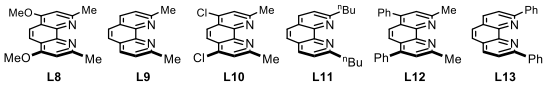


| $L_X$ | $Co(L_X)Br_2$ | | $Ni(L_X)Br_2$ | |
|---|---|---|---|---|
| | $E_{1/2}$ /V | $k_{obs}$ / $M^{-1}$ $s^{-1}$ | $E_{1/2}$ /V | $k_{obs}$ / $M^{-1}$ $s^{-1}$ |
| L8 | –1.52 | n.d.[a] | –1.14 | 43.8 0.8 |
| L9 | **1.37** | ***41.7 2.0*** | **1.08** | ***51.2 0.7*** |
| L10 | –1.28 | n.d.[a] | –1.02 | 43.8 0.8 |
| L11 | –1.40 | 73.9 3.4 | –1.06 | 6.52 0.66 |
| L12 | –1.35 | 36.2 0.8 | –1.08 | 32.9 0.4 |
| L13 | –1.31 | n.d.[a] | –0.95 | n.d.[a] |
| $M(L_9)Cl_2$ | –1.50 | 17.5 5.9 | –1.20 | 76.3 0.1 |

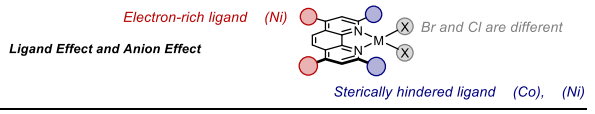


Kinetic rate constants (with **39**) and redox potentials (referenced to Fc/Fc$^+$) were measured and compared between nickel and cobalt complexes bearing different ligands. [a]Rate constants not determined due to uninterpretable CVs. Error bars were calculated on duplicated measurements.

**Transition State Calculation.** To corroborate the experimental and statistical modeling results, density functional theory (DFT) transition state analysis was performed. Aside from seeking a means to visualize the key intermediates, a goal was to survey the possibility of a radical-type pathway, which has been proposed in other Co(I)/Ni(I) systems (e.g., oxidative addition into alkyl halides).[28] An initial search of transition state geometries with allyl acetate was conducted and three different plausible pathways were located (Figure 6a). These transition states were categorized as (1) a coordination-ionization pathway (TS-1), (2) a coordinated radical-type pathway (TS-2), and (3) a non-coordinated radical-type pathway (TS-3). The Co and Ni complexes show similar patterns in the transition states (see supporting information, section 10) and here we used the Co($^{Me}$BPy) complex as an example.

As shown in Figure 6b, the geometry of the coordination-ionization transition state (TS-1) shared similar features with Pd(0) systems reported previously.[7] First, the distance between the metal and alkene (2.28 Å for Co–$C_{alkenyl}$ in Co($^{Me}$BPy) complex) shows a bonding interaction. Additionally, a bond is being formed between the metal and allylic carbon (2.20 Å for Co–$C_{allylic}$ in Co($^{Me}$BPy) complex) with concomitant bond dissociation between the allylic carbon and the acetate (2.73 Å for $C_{allylic}$–$O_{acetate}$ in Co($^{Me}$BPy) complex).

TS-2 and TS-3 (Figures 6b) show the radical abstraction of the acetate group by the metal. However, TS-2 also involves alkene coordination with the metal. Additionally, the trigonal-planer geometry (bond angles specified in Figure 6b for TS-2 and 3) of the allylic carbon supports the radical being generated at this position.

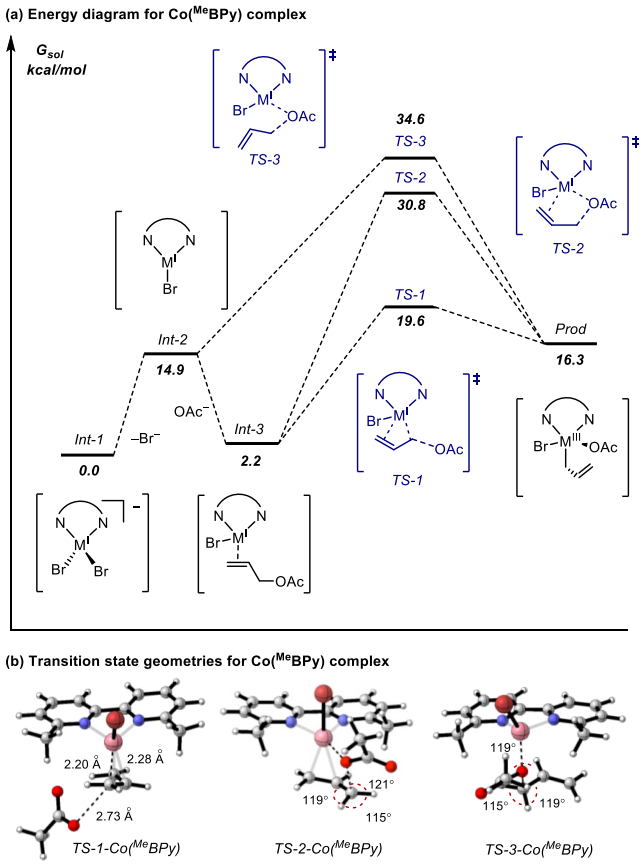


**Figure 6.** (a) Energy diagrams and (b) Geometries of transition states for Co($^{Me}$BPy) complex to exemplify. Transition state geometries and energies for other complexes are reported in supporting information (section 10).

Benchmark studies were conducted where we surveyed a combination of functionals and basis sets to calculate the activation free energy (see supporting information, section 10). In this process, three intermdiates were considered and their energies was tabulated in Figure 7a (Int-1: reduced M(I) complex, Int-2: Int-1 with a loss of bromide anion, and Int-3: Int-2 with coordination of allyl acetate). The (U)BP86-D3/DEF2-TZVPP, SMD(ACN) level of theory was found optimal since it matches the experimental derived activation

energy (Table 7). Through the comparison of the $\Delta G^{\ddagger}$ values, TS-2 and TS-3 are >6 kcal/mol higher than TS-1, which further supports the coordination-ionization pathway (TS-1) as the operating mechanism. This is consistent with both the experimental evidence derived from the Hammett and statistical modeling studies.

**Table 7. Experiment and computation-derived energies**

| *(kcal/mol)* | *Co($^{Me}$BPy)* | *Co($^{Me}$Phen)* | *Ni($^{Me}$BPy)* | *Ni($^{Me}$Phen)* |
|---|---|---|---|---|
| ***$G^{\ddagger}$(exp.)*** | ***20.6*** | ***20.0*** | ***19.9*** | ***19.6*** |
| ***$G^{\ddagger}$(TS-1)*** | *19.6* | *21.1* | *17.3* | *18.8* |
| ***$G^{\ddagger}$(TS-2)*** | *30.8* | *31.0* | *25.6* | *25.5* |
| ***$G^{\ddagger}$(TS-3)*** | *34.6* | *36.4* | *32.0* | *32.0* |

All energies are calculated at room temperature (298 K).

**Implications of the Kinetic Analysis on Catalysis.** Elucidating the kinetics of Co(I)/Ni(I) mediated oxidative addition has several implications in identifying the substrate/catalysts selection for the desired transformation. First, the mechanistic understanding provides a direct rationale between the $pK_a$ of the leaving group and the rate of oxidative addition (Figure 3d, and 7a). Moreover, our study demonstrate that C1 or C3 substituted allyllic electrophiles generate the same regioisomeric products irrespective of the substituents pattern (Table 4). However, the rate of oxidative addition for C1 and C3 substrates are different (e.g., **4** and **26**, **45** and **47,** Figure 7a), with C3 substituents reacting significantly faster than the C1 substituted allyl electrophiles. Therefore, if a faster oxidative addition rate is desired, substrates with a better leaving group and C3-substitution pattern should be utilized.

Although our study demonstrates that the oxidative addition mechanisms in Co and Ni systems are similar, we also noted a few differences. As depicted in Figure 7b, Co systems have a wider rate window than two Ni systems suggesting that the nickel complexes are relatively less sensitive to substrates' electronics (e.g., C3 and C4 substrates). Moreover, $^{Me}$Phen ligand is typically more reactive than $^{Me}$BPy ligand. Therefore, if a faster oxidative addition rate is preferred, Ni($^{Me}$Phen) could be utilized for the C4−substrates, while Co($^{Me}$Phen) could be beneficial for the C3−substrates. Furthermore, evaluation of ligand features indicate a faster oxidative addition that uses an electron-rich ligand with less sterics (Table 5).

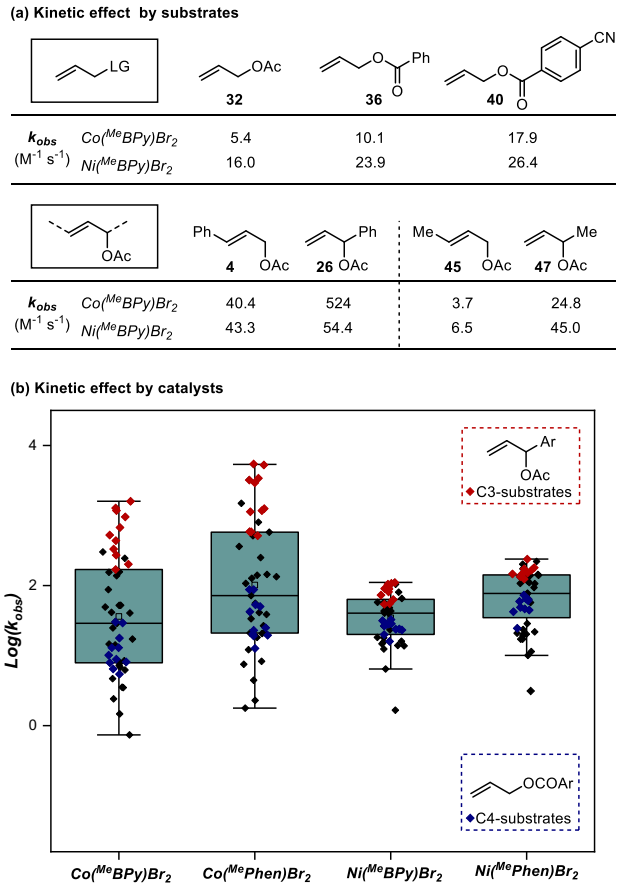


**Figure 7.** Kinetic effect by (a) substrates and (b) catalysts.

## Conclusion

In this study, we present a mechanistic investigation of a catalytically relevant Co(I)/Ni(I) mediated oxidative addition process. The reactivity was initially surveyed by cyclic voltammetry and bulk electrolysis reactions. Kinetics were investigated through Hammett-type, statistical modeling, and DFT studies. These studies led to the hypothesis of a coordination-ionization type mechanism similar to what was proposed for Pd(0)-mediated oxidative addition in Tsuji-Trost reactions. A kinetic study of the substituted allylic substrates further solidified the similarity between Co(I)/Ni(I) and Pd(0) systems. Additionally, through comparison of oxidative addition rates of different Co/Ni complexes, ligand electronic/steric effects were investigated. We envision the mechanistic insight gained in this study should guide the design of new catalysis, which will be reported in due course.

# ASSOCIATED CONTENT

## Data Availability Statement

The data that support the findings in this work are available within the paper and Supporting Information.

## Supporting Information

The Supporting Information is available free of charge on the ACS Publications website.

Materials and methods, experimental cyclic voltammograms and kinetic data, parameters used in the modeling, bulk electrolysis conditions and results, computational details, characterization data

and spectra for synthesizing metal complexes, ligands and substrates, and coordinates of DFT-optimized structures. (PDF)

## AUTHOR INFORMATION

### Corresponding Authors

*sigman@chem.utah.edu

### Notes

The authors declare no competing financial interest.

## ACKNOWLEDGMENT

The authors would like to thank the National Science Foundation Center for Synthetic Organic Electrochemistry for funding CHE-2002158). NMR results included in this report were recorded at the David M. Grant NMR Center, a University of Utah Core Facility. Funds for the construction of the Center and the helium recovery system were obtained from the University of Utah and the National Institutes of Health awards 1C06RR017539- 01A1 and 3R01GM063540-17W1, respectively. NMR instruments were purchased with the support of the University of Utah and the National Institutes of Health award 1S10OD25241-01.

## REFERENCES

(1) For selected reviews, see: (a) Lu, Z.; Ma, S. Metal-Catalyzed Enantioselective Allylation in Asymmetric Synthesis. *Angew. Chem. Int. Ed Engl.* **2008**, *47* (2), 258–297. (b) Trost, B. M.; Crawley, M. L. Asymmetric Transition-Metal-Catalyzed Allylic Alkylations: Applications in Total Synthesis. *Chem. Rev.* **2003**, *103* (8), 2921–2944. (c) Han, J.-F.; Guo, P.; Zhang, X.-G.; Liao, J.-B.; Ye, K.-Y. Recent Advances in Cobalt-Catalyzed Allylic Functionalization. *Org. Biomol. Chem.* **2020**, *18* (39), 7740–7750. (d) Pàmies, O.; Margalef, J.; Cañellas, S.; James, J.; Judge, E.; Guiry, P. J.; Moberg, C.; Bäckvall, J.-E.; Pfaltz, A.; Pericàs, M. A.; Diéguez, M. Recent Advances in Enantioselective Pd-Catalyzed Allylic Substitution: From Design to Applications. *Chem. Rev.* **2021**, *121* (8), 4373–4505.

(2) For selected reviews, see: (a) Huang, H.-M.; Bellotti, P.; Glorius, F. Transition Metal-Catalysed Allylic Functionalization Reactions Involving Radicals. *Chem. Soc. Rev.* **2020**, *49* (17), 6186–6197. (b) Spielmann, K.; Niel, G.; de Figueiredo, R. M.; Campagne, J.-M. Catalytic Nucleophilic "umpoled" π-Allyl Reagents. *Chem. Soc. Rev.* **2018**, *47* (4), 1159–1173.

(3) Selected synthetic studies in Co-catalyzed reductive allylation reactions: (a) Gosmini, C.; Gomes, P.; Périchon, J. Allylation of Carbonyl Compounds by Allylic Acetates Using a Cobalt Halide as Catalyst. *Synthesis* **2003**, 12, 1909–1915. (b) Qian, X.; Auffrant, A.; Felouat, A.; Gosmini, C. Cobalt-Catalyzed Reductive Allylation of Alkyl Halides with Allylic Acetates or Carbonates. *Angew. Chem. Int. Ed.* **2011**, *123* (44), 10586–10589. (c) Shi, C.; Li, F.; Chen, Y.; Lin, S.; Hao, E.; Guo, Z.; Wosqa, U. T.; Zhang, D.; Shi, L. Photocatalytic Umpolung Synthesis of Nucleophilic π-Allylcobalt Complexes for Allylation of Aldehydes. *ACS Catal.* **2021**, *11* (5), 2992–2998. (d) Gualandi, A.; Rodeghiero, G.; Perciaccante, R.; Jansen, T. P.; Moreno-Cabrerizo, C.; Foucher, C.; Marchini, M.; Ceroni, P.; Cozzi, P. G. Catalytic Photoredox Allylation of Aldehydes Promoted by a Cobalt Complex. *Adv. Synth. Catal.* **2021**, *363* (4), 1105–1111. (e) Wang, L.; Wang, L.; Li, M.; Chong, Q.; Meng, F. Cobalt-Catalyzed Diastereo- and Enantioselective Reductive Allyl Additions to Aldehydes with Allylic Alcohol Derivatives via Allyl Radical Intermediates. *J. Am. Chem. Soc.* **2021**, *143* (32), 12755–12765. (f) Cristòfol, À.; Limburg, B.; Kleij, A. W. Expedient Dual Co/Organophotoredox Catalyzed Stereoselective Synthesis of All-carbon Quaternary Centers. *Angew. Chem. Int. Ed.* **2021**, *60* (28), 15266–15270. (g) Xue, S.; Cristòfol, À.; Limburg, B.; Zeng, Q.; Kleij, A. W. Dual Cobalt/Organophotoredox Catalysis for Diastereo- and Regioselective 1,2-Difunctionalization of 1,3-Diene Surrogates Creating Quaternary Carbon Centers. *ACS Catal.* **2022**, *12* (6), 3651–3659.

(4) Selected synthetic studies in Ni-catalyzed reductive allylation reactions: (a) Tan, Z.; Wan, X.; Zang, Z.; Qian, Q.; Deng, W.; Gong, H. Ni-Catalyzed Asymmetric Reductive Allylation of Aldehydes with Allylic Carbonates. *Chem. Commun.* **2014**, *50* (29), 3827–3830. (b) Moragas, T.; Cornella, J.; Martin, R. Ligand-Controlled Regiodivergent Ni-Catalyzed Reductive Carboxylation of Allyl Esters with $CO_2$. *J. Am. Chem. Soc.* **2014**, *136* (51), 17702–17705. (c) Gualandi, A.; Rodeghiero, G.; Faraone, A.; Patuzzo, F.; Marchini, M.; Calogero, F.; Perciaccante, R.; Jansen, T. P.; Ceroni, P.; Cozzi, P. G. Allylation of Aldehydes by Dual Photoredox and Nickel Catalysis. *Chem. Commun.* **2019**, *55* (48), 6838–6841. (d) Ye, Y.; Qi, X.; Xu, B.; Lin, Y.; Xiang, H.; Zou, L.; Ye, X.-Y.; Xie, T. Nickel-Catalyzed Cross-Electrophile Allylation of Vinyl Bromides and the Modification of Anti-Tumour Natural Medicine β-Elemene. *Chem. Sci.* **2022**, *13* (23), 6959–6966. (e) Calogero, F.; Potenti, S.; Bassan, E.; Fermi, A.; Gualandi, A.; Monaldi, J.; Dereli, B.; Maity, B.; Cavallo, L.; Ceroni, P.; Cozzi, P. G. Nickel-Mediated Enantioselective Photoredox Allylation of Aldehydes with Visible Light. *Angew. Chem. Int. Ed.* **2022**, *61* (11), e202114981. (f) Fan, Z.; Chen, S.; Zou, S.; Xi, C. Direct C–C Bond Formation of Allylic Alcohols with $CO_2$ toward Carboxylic Acids by Photoredox/Nickel Dual Catalysis. *ACS Catal.* **2022**, *12* (5), 2781–2787. (g) Diallo, A. G.; Paris, D.; Faye, D.; Gaillard, S.; Lautens, M.; Renaud, J.-L. Dual Ni/Organophotoredox Catalyzed Allylative Ring Opening Reaction of Oxabenzonorbornadienes and Analogs. *ACS Catal.* **2022**, *12* (6), 3681–3688.

(5) Hartwig, J. F. Allylic Substitution. In *Organotransition Metal Chemistry: From Bonding to Catalysis*; Murdzek, J., Eds.; University Science Books:Columbia, MD, **2010**; pp 974−977.

(6) (a) Yamamoto, T.; Saito, O.; Yamamoto, A. Oxidative Addition of Allyl Acetate to Palladium(0) Complexes. *J. Am. Chem. Soc.* **1981**, *103* (18), 5600–5602. (b) Yamamoto, T.; Akimoto, M.; Saito, O.; Yamamoto, A. Interaction of Palladium(0) Complexes with Allylic Acetates, Allyl Ethers, Allyl Phenyl Chalcogenides, Allylic Alcohols, and Allylamines. Oxidative Addition, Condensation, Disproportionation, and π-Complex Formation. *Organometallics* **1986**, *5* (8), 1559–1567.

(7) Selected DFT studies on Pd(0) mediated oxidative addition into allyl esters: (a) Tang, D.; Luo, X.; Shen, W.; Li, M. The Mechanism of Enantioselective Palladium(0)-Catalyzed Allylic Alkylation with Chiral Oxazolinylpyridines: A DFT Study. *Theochem* **2005**, *716* (1–3), 79–87. (b) Pohorilets, I.; Tracey, M. P.; LeClaire, M. J.; Moore, E. M.; Lu, G.; Liu, P.; Koide, K. Kinetics and Inverse Temperature Dependence of a Tsuji–Trost Reaction in Aqueous Buffer. *ACS Catal.* **2019**, *9* (12), 11720–11733. (c) Cusumano, A. Q.; Stoltz, B. M.; Goddard, W. A. Reaction Mechanism, Origins of Enantioselectivity, and Reactivity Trends in Asymmetric Allylic Alkylation: A Comprehensive Quantum Mechanics Investigation of a $C(Sp^3)$-$C(Sp^3)$ Cross-Coupling. *J. Am. Chem. Soc.* **2020**, *142* (32), 13917–13933.

(8) (a) Osakada, K.; Chiba, T.; Nakamura, Y.; Yamamoto, T.; Yamamoto, A. Steric Effect of Substituents in Allylic Groups in Oxidative Addition of Allylic Phenyl Sulphides to a Palladium(0) Complex. C–S Bond Cleavage Triggered by Attack of Pd on the Terminal Carbon of the C–C Double Bond. *J. Chem. Soc. Chem. Commun*. **1986**, No. 21, 1589–1591. (b) Kurosawa, H.; Kajimaru, H.; Ogoshi, S.; Yoneda, H.; Miki, K.; Kasai, N.; Murai, S.; Ikeda, I. Novel Syn Oxidative Addition of Allylic Halides to Olefin Complexes of Palladium(0) and Platinum(0). *J. Am. Chem. Soc*. **1992**, *114* (22), 8417–8424.

(9) (a) Agenet, N.; Amatore, C.; Gamez, S.; Gérardin, H.; Jutand, A.; Meyer, G.; Orthwein, C. Effect of the Leaving Group and the Allylic Structure on the Kinetics and Thermodynamics of the Reaction of Allylic Carboxylates with Palladium(0) Complexes. *ARKIVOC* **2002**(5), 92–101. (b) Gumrukcu, Y.; de Bruin, B.; Reek, J. A Mechanistic Study of Direct Activation of Allylic Alcohols in Palladium Catalyzed Amination Reactions. *Catalysts* **2015**, *5* (1), 349–365.

(10) (a) Amatore, C.; Gamez, S.; Jutand, A.; Meyer, G.; Moreno-Manas, M.; Morral, L.; Pleixats, R. Oxidative Addition of Allylic Carbonates to Palladium(0) Complexes: Reversibility and Isomerization. *Chemistry* **2000**, *6* (18), 3372–3376. (b) Hayashi, T.; Yamamoto, A.; Hagihara, T. Stereo- and Regiochemistry in Palladium-Catalyzed Nucleophilic Substitution of Optically Active (E)- and (Z)-Allyl Acetates. *J. Org. Chem*. **1986**, *51* (5), 723–727.
(11) Evans, L. A.; Fey, N.; Harvey, J. N.; Hose, D.; Lloyd-Jones, G. C.; Murray, P.; Orpen, A. G.; Osborne, R.; Owen-Smith, G. J. J.; Purdie, M. Counterintuitive Kinetics in Tsuji-Trost Allylation: Ion-Pair Partitioning and Implications for Asymmetric Catalysis. *J. Am. Chem. Soc.* **2008**, *130* (44), 14471–14473.
(12) (a) Gomes, P.; Buriez, O.; Labbé, E.; Gosmini, C.; Périchon, J. Mechanism(s) of the Cobalt-Catalyzed Electrochemical Coupling between Aromatic Halides and Allylic Acetates. *J. Electroanal. Chem*. **2004**, *562* (2), 255–260. (b) Limburg, B.; Cristòfol, À.; Kleij, A. W. Decoding Key Transient Inter-Catalyst Interactions in a Reductive Metallaphotoredox- Catalyzed Allylation Reaction. *J. Am. Chem. Soc.* **2022**, *144* (24), 10912–10920.
(13) Matsui, J. K.; Gutiérrez-Bonet, Á.; Rotella, M.; Alam, R.; Gutierrez, O.; Molander, G. A. Photoredox/Nickel-Catalyzed Single-Electron Tsuji-Trost Reaction: Development and Mechanistic Insights. *Angew. Chem. Int. Ed.* **2018**, *57* (48), 15847–15851.
(14) (a) Diccianni, J. B.; Katigbak, J.; Hu, C.; Diao, T. Mechanistic Characterization of (Xantphos)Ni(I)-Mediated Alkyl Bromide Activation: Oxidative Addition, Electron Transfer, or Halogen-Atom Abstraction. *J. Am. Chem. Soc*. **2019**, *141* (4), 1788–1796. (b) Lin, Q.; Diao, T. Mechanism of Ni-Catalyzed Reductive 1,2-Dicarbofunctionalization of Alkenes. *J. Am. Chem. Soc.* **2019**, *141* (44), 17937–17948. (c) Ting, S. I.; Williams, W. L.; Doyle, A. G. Oxidative Addition of Aryl Halides to a Ni(I)-Bipyridine Complex. *J. Am. Chem. Soc.* **2022**, *144* (12), 5575–5582.
(15) (a) Hickey, D. P.; Sandford, C.; Rhodes, Z.; Gensch, T.; Fries, L. R.; Sigman, M. S.; Minteer, S. D. Investigating the Role of Ligand Electronics on Stabilizing Electrocatalytically Relevant Low-Valent Co(I) Intermediates. *J. Am. Chem. Soc.* **2019**, *141*, 1382–1392. (b) Sandford, C.; Fries, L. R.; Ball, T. E.; Minteer, S. D.; Sigman, M. S. Mechanistic Studies into the Oxidative Addition of Co(I) Complexes: Combining Electroanalytical Techniques with Parameterization. *J. Am. Chem. Soc.* **2019**, *141*, 18877–18889.
(16) (a) Tang, T.; Sandford, C.; Minteer, S. D.; Sigman, M. S. Analyzing mechanisms in Co(I) redox catalysis using a pattern recognition platform. *Chem. Sci.* **2021**, *12*, 4771–4778. (b) Tang, T.; Friede, N. C.; Minteer, S. D.; Sigman, M. S. Comparing Halogen Atom Abstraction Kinetics for Mn(I), Fe(I), Co(I), and Ni(I) Complexes by Combining Electroanalytical and Statistical Modeling. *European J. Org. Chem.* **2022**, e202200064.
(17) Sandford, C.; Edwards, M. A.; Klunder, K. J.; Hickey, D. P.; Li, M.; Barman, K. Sigman, M. S.; White, H. S.; Minteer, S. D. A synthetic chemist's guide to electroanalytical tools for studying reaction mechanisms. *Chem. Sci.* **2019**, *10*, 6404–6422.
(18) Lin, Q.; Fu, Y.; Liu, P.; Diao, T. Monovalent Nickel-Mediated Radical Formation: A Concerted Halogen-Atom Dissociation Pathway Determined by Electroanalytical Studies. *J. Am. Chem. Soc*. **2021**, *143* (35), 14196–14206.
(19) Selected studies in Co and Ni-catalyzed reductive coupling reactions: (a) Gnaim, S.; Bauer, A.; Zhang, H.-J.; Chen, L.; Gannett, C.; Malapit, C. A.; Hill, D. E.; Vogt, D.; Tang, T.; Daley, R. A.; Hao, W.; Zeng, R.; Quertenmont, M.; Beck, W. D.; Kandahari, E.; Vantourout, J. C.; Echeverria, P.-G.; Abruna, H. D.; Blackmond, D. G.; Minteer, S. D.; Reisman, S. E.; Sigman, M. S.; Baran, P. S. Cobalt-Electrocatalytic HAT for Functionalization of Unsaturated C-C Bonds. *Nature* **2022**, *605* (7911), 687–695. (b) Nogi, K.; Fujihara, T.; Terao, J.; Tsuji, Y. Cobalt- and Nickel-Catalyzed Carboxylation of Alkenyl and Sterically Hindered Aryl Triflates Utilizing $CO_2$. *J. Org. Chem.* **2015**, *80* (22), 11618–11623. (c) Shrestha, R.; Dorn, S. C. M.; Weix, D. J. Nickel-Catalyzed Reductive Conjugate Addition to Enones via Allylnickel Intermediates. *J. Am. Chem. Soc.* **2013**, *135* (2), 751–762. (d) Kumar, G. S.; Peshkov, A.; Brzozowska, A.; Nikolaienko, P.; Zhu, C.; Rueping, M. Nickel-Catalyzed Chain-Walking Cross-Electrophile Coupling of Alkyl and Aryl Halides and Olefin Hydroarylation Enabled by Electrochemical Reduction. *Angew. Chem. Int. Ed*. **2020**, *59* (16), 6513–6519. (e) Jiao, K.-J.; Ma, C.; Liu, D.; Qiu, H.; Cheng, B.; Mei, T.-S. Nickel-Catalyzed Electrochemical Reductive Relay Cross-Coupling of Alkyl Halides with Alkyl Carboxylic Acids. *Org. Chem. Front.* **2021**, *8* (23), 6603–6608. (f) Davies, J.; Janssen-Müller, D.; Zimin, D. P.; Day, C. S.; Yanagi, T.; Elfert, J.; Martin, R. Ni-Catalyzed Carboxylation of Aziridines En Route to β-Amino Acids. *J. Am. Chem. Soc.* **2021**, *143* (13), 4949–4954. (g) Yang, Y.-Z.; Li, Y.; Lv, G.-F.; He, D.-L.; Li, J.-H. Nickel-Catalyzed C-S Reductive Cross-Coupling of Alkyl Halides with Arylthiosilanes toward Alkyl Aryl Thioethers. *Org. Lett*. **2022**, *24* (28), 5115–5119.
(20) (a) Marshall, W. J.; Grushin, V. V. Activation of Chlorobenzene with Ni(0) N,N-Chelates – A Remarkably Profound Effect of a Minuscule Change in Ligand Structure. *Can. J. Chem.* **2005**, *83* (6–7), 640–645. (b) Powers, D. C.; Anderson, B. L.; Nocera, D. G. Two-Electron HCl to H2 Photocycle Promoted by Ni(II) Polypyridyl Halide Complexes. *J. Am. Chem. Soc*. **2013**, *135* (50), 18876–18883. (c) Biswas, S.; Weix, D. J. Mechanism and Selectivity in Nickel-Catalyzed Cross-Electrophile Coupling of Aryl Halides with Alkyl Halides. *J. Am. Chem. Soc*. **2013**, *135* (43), 16192–16197. (d) Shirvan, S. A., Haydari Dezfuli, S., Khazali, F., Aghajeri M., Borsalani, A. *Acta Cryst.* **2012**, *E68*, m1363. (e) Akbarzadeh-T, N.; Rezvani, A.; Saravani, H.; Kondori, T.; Amani, V.; Khavasi, H. R. Synthesis, Characterization, and Crystal Structure of New Four-Coordinated Cobalt(II) Complexes Containing Phenanthroline Derivatives. *Res. Chem. Intermed*. **2015**, *41* (3), 1247–1256.
(21) Wang, Z.-J.; Zheng, S.; Romero, E.; Matsui, J. K.; Molander, G. A. Regioselective Single-Electron Tsuji-Trost Reaction of Allylic Alcohols: A Photoredox/Nickel Dual Catalytic Approach. *Org. Lett.* **2019**, *21* (16), 6543–6547.
(22) Hansch, C.; Leo, A.; Taft, R. W. A survey of Hammett substituent constants and resonance and field parameters. *Chem. Rev.* **1991**, *91*, 165–195.
(23) Carrion, F.; Dewar, M. J. S. Ground States of Molecules. 59. MNDO Study of $SN_2$ Reactions and Related Processes. *J. Am. Chem. Soc*. **1984**, *106* (12), 3531–3539.
(24) Tinnermann, H.; Sung, S.; Csókás, D.; Toh, Z. H.; Fraser, C.; Young, R. D. Alkali Metal Adducts of an Iron(0) Complex and Their Synergistic FLP-Type Activation of Aliphatic C-X Bonds. *J. Am. Chem. Soc.* **2021**, *143* (28), 10700–10708.
(25) (a) Santerre, G. M.; Hansrote, C. J., Jr; Crowell, T. I. The Reaction of Aromatic Aldehydes with N-Butylamine. Acid Catalysis and Substituent Effects1. *J. Am. Chem. Soc*. **1958**, *80* (5), 1254–1257. (b) Hancock, C. K.; Idoux, J. P. Quantitative Solubility-Structure Relations for Some Meta- and Para-Substituted Benzoic Acids in p-Dioxane and Tetrahydrofuran. *J. Org. Chem.* **1967**, *32* (6), 1931–1934.
(26) Till, N. A.; Oh, S.; MacMillan, D. W. C.; Bird, M. J. The Application of Pulse Radiolysis to the Study of Ni(I) Intermediates in Ni-Catalyzed Cross-Coupling Reactions. *J. Am. Chem. Soc.* **2021**, *143* (25), 9332–9337.
(27) A similar transition state was reported for Ni(0) mediated processes. For selected studies on Ni(0) mediated oxidative addition into allyl substrates, see (a) Yamamoto, T.; Ishizu, J.; Yamamoto, A. Interaction of Nickel(0) Complexes with Allyl Carboxylates, Allyl Ethers, Allylic Alcohols, and Vinyl Acetate. π-Complex Formation and Oxidative Addition to Nickel Involving Cleavage of the Alkenyl-Oxygen Bond. *J. Am. Chem. Soc*. **1981**, *103* (23), 6863–6869. (b) Bottoni, A.; Miscione, G. P.; Novoa, J. J.; Prat-Resina, X. DFT Computational Study of the Mechanism of Allyl Halides Carbonylation Catalyzed by Nickel Tetracarbonyl. *J. Am. Chem. Soc*. **2003**, *125* (34), 10412–10419. (c) Egiazaryan, K. T.; Shamsiev, R. S.; Flid, V. R. Quantum chemical investigation of the oxidative addition reaction of allyl carboxylates to Ni(0) and Pd(0) complexes. *Fine Chemical Technologies.* **2020**, *14* (6), 56–65.
(28) For selected reviews, see (a) Choi, J.; Fu, G. C. Transition Metal-Catalyzed Alkyl-Alkyl Bond Formation: Another Dimension in Cross-Coupling Chemistry. *Science* **2017**, *356* (6334), eaaf7230. (b) Diccianni, J. B.; Diao, T. Mechanisms of Nickel-Catalyzed Cross-Coupling Reactions. *Trends in Chemistry* **2019**, *1* (9), 830–844. (c)

Cahiez, G.; Moyeux, A. Cobalt-Catalyzed Cross-Coupling Reactions. *Chem. Rev.* **2010**, *110* (3), 1435–1462.
(29) (a) Harper, K. C.; Sigman, M. S. Using Physical Organic Parameters To Correlate Asymmetric Catalyst Performance. *J. Org. Chem.* **2013**, *78*, 2813–2818. (b) Sigman, M. S.; Harper, K. C.; Bess, E. N.; Milo, A. The Development of Multidimensional Analysis Tools for Asymmetric Catalysis and Beyond. *Acc. Chem. Res.* **2016**, 49, 1292–1301.
(30) Yamaguchi, E.; Itoh, A.; Suzuki, H. Nickel-Catalyzed Reductive Allylation of Aldehydes with Allyl Acetates. *Synthesis* **2021**, *53* (08), 1489–1494.